IET Generation, Transmission & Distribution

Special Issue on Power Electronic Converter Systems for Integration of Renewable Energy Sources

IET Journals
The Institution of Engineering and Technology

Balanced and unbalanced inverter strategies in battery storage systems for low-voltage grid support

ISSN 1751-8687
Received on 14th April 2014
Revised on 30th October 2014
Accepted on 7th April 2015
doi: 10.1049/iet-gtd.2014.0341
www.ietdl.org

Frederik Geth ✉, *Jeroen Tant*, *Ronnie Belmans*, *Johan Driesen*

Department of Electrical Engineering (ESAT), ELECTA, University of Leuven (KU Leuven), Leuven, Belgium and Energyville, Genk, Belgium

✉ *E-mail: frederik.geth@esat.kuleuven.be*

Abstract: The design of battery storage systems includes technology choices for the batteries and for the inverter. The impact of the inverter design on the optimal design and operation of the storage system has not been analysed before. Therefore four inverter designs are compared with this research. The most basic inverter model assumes only symmetric active power exchange; the most advanced inverter model allows interphase active power transfer and reactive power control. A multi-objective optimisation method is used, to visualise the trade-offs between two technical objective functions for cycling control – voltage regulation and peak power reduction – for a given annual cost. The method is applied to a real-world scenario, based on an existing feeder in a residential part of a city in Flanders, Belgium. Internal losses and losses in the grid are quantified for the different designs. Modelling a battery storage system purely as a finite source/sink of active power in a low-voltage grid, strongly underestimates the potential because of the existing phase unbalance. Counteracting phase unbalance through an inter-phase power transfer capable inverter, even more so than adding reactive power control, improves the performance of battery storage systems.

1 Introduction

Storage is considered a key technology in the evolution of the power system [1]. Storage can facilitate much larger deployment of intermittent renewable energy sources (RES) [2]. It represents a source of operational flexibility that can help to avoid curtailment of RES at high penetration [3]. Low cost distributed storage is considered one of the drivers to transform the power system infrastructure [2].

In general, current storage technology options have not proven truly effective for substantial and widely applicable deployment [2]. Nevertheless, specific niches have come forward, which explains the deployment throughout the world [4] of geographically-limited pumped hydro storage (PHS). Other storage technologies improve on the limiting characteristics of PHS and are therefore often considered in planning studies for future application in the power system [1]. However, it remains difficult to justify investment in storage units for single-service operation. A combination of multiple services may improve the business case [5, 6]. Storage operation can be performed with multiple objectives: different services can be provided at different times or even at the same time [7–9]. Moreover, storage design and sizing can be considered with multiple objectives, as trade-off solutions can be chosen to match different services and changing applications throughout the lifetime of the unit. Insight in the design, sizing and cost of multi-objective storage systems is crucial to facilitate a wider deployment.

In planning methodologies, a number of storage-related problems are addressed, for example, for battery storage the design, sizing, control and cost. The design selection problem considers multiple choices for the system components and system topology. Next, sizing is the determination of the actual rating of the components chosen in the design problem. To assess the sizing, the operation of the system is to be simulated [10, 11].

The goal of this research is to assess the importance of inverter design in battery energy storage systems (BESSs). For different designs, the trade-offs between different objectives are studied: voltage regulation at the in-house connection terminals, total peak power reduction and annual BESS cost. The analysis is performed for a currently operating low-voltage (LV) grid that is starting to show problems caused by increased electricity consumption and increased penetration of local RES. BESS internal losses and BESS-caused losses in the grid are examined. As in [12], storage-supplied services are used to maintain normal grid operation, mitigating the impact of any energy producing or consuming resources, at the lowest possible cost. Conversely, the goal is *not* to support, the sources of the disturbances explicitly, as, for example, supporting wind power integration through storage in [13].

The paper is structured as follows. First, a literature review of storage planning methodologies for distribution grids is given. Then, a scenario of a residential feeder located in a city in Flanders, Belgium, is developed. Finally, the optimal BESS design and sizing results in this grid are presented.

2 Storage in distribution grids

A BESS consists of batteries with a bidirectional grid interface and a control system. Owing to the intrinsic modularity of battery cells and the wide range of chemistries, BESSs are considered versatile and easily scalable from kW/kWh to MW/MWh size, as shown in examinations of numerous projects [14]. To assess the many available battery chemistries, numerous parameters are considered charging efficiency, capacity, power rating, self-discharge, specific costs and so on. For example, Li-ion is considered an attractive option for LV grid application, given its relatively high energy density, attractive cycle life and high efficiency. However, the prices are high, but because of the substantial development and experience gained with Li-ion batteries in electric vehicles, a substantial price decrease is expected in the near term [4].

The storage control problem, namely determining an optimal charge and discharge schedule to support a certain objective, has been discussed in the literature for a long time because of the classic arbitrage control of PHS. The sizing of storage of different technologies can be optimised for cost–benefit in a unit commitment context, while including lifetime estimation [15]. The power system

integration of BESSs poses specific questions, mainly related to cost-optimal cycling because of the battery wear and lifetime.

Grid interface technology is crucial for cost-effective BESSs. At least, an efficient and bidirectional active power grid interface is required, allowing for charging and discharging the batteries. Such interface is considered similar to a photovoltaic (PV) inverter in terms of hardware and control [16]. As reactive power control in PV inverters [7] is considered crucial to further the deployment of PV in medium-voltage (MV) and LV grids [17, 18], it sometimes is examined as well for BESS [17, 19]. For example, in [19], a BESS is operated to maximise a profit, while mitigating voltage deviations through both active and reactive powers. The BESS cycling is, however, limited to a maximum of one cycle per day. The relationship of grid losses and the optimal sizing and siting of storage is analysed in MV grids [20], but only for a balanced grid situation. Furthermore, inter-phase power transfer capable configurations are developed [21], and the application in BESS is modelled in [9]. Since aggregation related advantages, dedicated BESSs in the LV grid can more efficiently manage the problems caused by the variability of loads and RES [22].

In the literature, the interplay between grid phase unbalance and inverter design in BESS has not been analysed. Furthermore, it is unknown, both for single and multiservice operation, how inverter capabilities change the optimal sizing of BESS. Finally, limits on cycling are often imposed to avoid battery depreciation rate variability, thereby potentially underestimating the efficacy of the system towards technical objectives considered.

3 Scenario

The scenario uses a 230/400 V reference grid with the TT earthing arrangement [23] based on the topology of a real feeder in a city in Flanders, Belgium. This case study is performed to study the feasibility of a BESS for grid support, as it is difficult to install a larger transformer because of the space limitations. Furthermore, it is expensive to replace underground cables in the urban environment.

A schematic representation of this three-phase distribution feeder with underground four-wire cables is shown in Fig. 1. This topology, provided by a Flemish DSO, has 29 branches towards buildings with a total of 39 individual household connections. The feeder cable type is EIAJB 1 kV 3×70 mm^2 1×50 mm^2 Cu. The connection cable from the feeder to the building terminal is 8 m in length, type EAXVB 1 kV 4×16 mm^2 Cu, except for the one to building 28 which has a cross section of 35 mm^2. Cable impedances and current limits J_c^{nom} are given in Table 1. Each individual household is assumed to have a single-phase connection between one phase and the neutral conductor, with a nominal line-to-neutral voltage U_{nom} of 230 V. Cable impedance values are calculated according to design specifications in the Belgian standard for underground distribution cables NBN C33-322 [24]. Cable current limits J_l^{nom}, for all conductors including the neutral, are taken into account. A 100 kVA, 10/0.4 kV transformer is assumed with an impedance of $0.0532 + 0.1692\text{j}\ \Omega$ with a varying voltage at the MV side. To avoid under voltage, the transformer is operating at a tap stand of 233 V. The normally distributed MV side voltage variations result in a standard deviation of the no-load voltage at the LV side of 1.1 V. For consumer connections in this grid, X and R are of the same order of magnitude, so both active and reactive powers can control the voltage [25].

Table 1 Cable parameters at 45°C

Cable description	Impedance, Ω/km	J_l^{nom}, A
EAXVB 1 kV 4×16 mm^2 Al	$1.265 + 0.083\text{j}$	90
EAXVB 1 kV 4×35 mm^2 Al	$0.576 + 0.081\text{j}$	140
EIAJB 1 kV 3×70 mm^2, 1×50 mm^2 Cu	$0.295 + 0.085\text{j}$	250

Within the LINEAR project [26], a large set of household electricity consumption profiles measured in 2007 is available, with a time step T_s of 15 min. For Flanders statistically representative set $\mathcal{H}_0$ containing 39 profiles is sampled [27], using the profiles which were self-identified in the survey as within the 'urban' environment as opposed to 'rural'. Average household

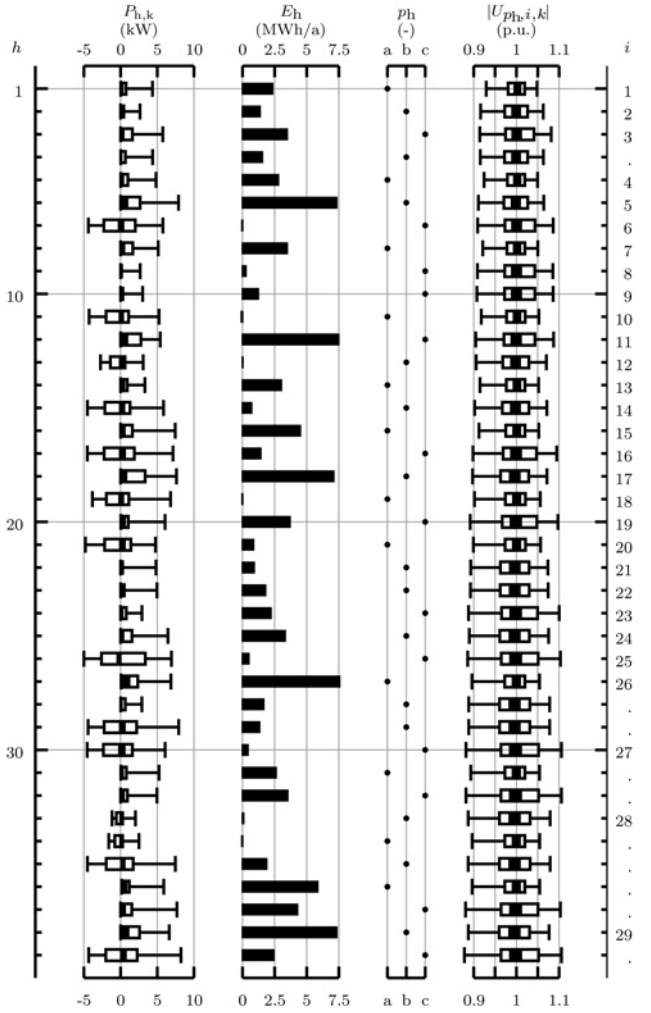

Fig. 2 *Load scenario definition with properties of the 39 single-phase individual households h at grid connections i: power profile box plot (column 1), annual energy consumption (column 2), the phase the profile is connected to (column 3) and the voltage magnitude box plot in that phase (column 4)*

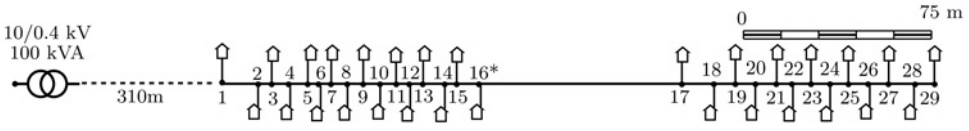

Fig. 1 *Schematic diagram of the feeder used in the scenario with 29 connections i*

BESS location marked at i = 16

Cable lengths are drawn to scale

consumption (without PV) is 3913 kWh/a. Detailed statistics of the household profiles are shown in Fig. 2 in columns 1 and 2. A modified box plot is used to display the distribution of time profiles. An additional box, spanning the 5–95th percentiles, is added to the standard box plot in order to emphasise peak values. A constant power load model with a unity power factor is assumed. Houses with negative power peaks have a rooftop PV installation, limited to a maximum of 5 kVA. A randomised phase is assigned. In some dwellings, there are multiple contracted parties (e.g. apartment), hence 39 profiles are used for the 29 load connection points i depicted in Fig. 1. Each individual household h has a current limit of $I_h^{\text{nom}} = 40$ A.

A load flow method for three-phase unbalanced radial grids is implemented in MATLAB, based on the backward–forward sweep technique [28], and is solved to a numerical accuracy of 1 μV. The voltage distribution at the terminal connection points in the households is depicted in column 3 of Fig. 2. The annual extreme voltages are outside of ±10% around U_{nom}. Therefore the load flow results are not in compliance with EN50160 standard [29] because of voltages being too high. The grid energy loss $E_{\text{loss}}^{\text{grid}}$ equals 3.5 MWh/a. The dynamic electricity tariff m_k as defined in [9] is imposed. At these prices, the cost of the grid losses is 642 €/a. In comparison, the annual cost of all electricity consumed by the 39 households in the scenario feeder, without PV, is equal to 27.4 k€/a.

In this paper, the BESS annual cost is fixed at 5000 €/a and the BESS location is fixed: connected directly to the feeder at the connection $i = 16$ in Fig. 1. A sensitivity analysis with respect to annual cost, battery technology and location is provided in previous work [9].

4 BESS model

In this section, model [9] is extended; the full description of the original model is provided in [9].

4.1 Original model

The decision variables for design are the nominal inverter apparent power rating $S_{\text{nom}}^{\text{inv}}$, the nominal battery capacity E_{nom}, the effective battery capacity E_{eff} and the nominal dc bus power rating $P_{\text{nom}}^{\text{dc}}$. The decision variables for control describe the power flow at each time step k through each phase p of the inverter: $S_{p,k}^{\text{inv}} = P_{p,k}^{\text{inv}} + \text{j}Q_{p,k}^{\text{inv}}$. The battery energy content E_k, the battery discharge power P_k^{d} and the charge power P_k^{c} are auxiliary decision variables. These variables are used within the cost model, where they determine the components for battery depreciation cost $K_{\text{depr}}^{\text{bat}}$ (a variable cost), energy cost K_{E} (a variable cost) and fixed cost K_{fix} (includes inverter depreciation, BESS maintenance and capital costs) in the total annual BESS cost K_{BESS}

$$K_{\text{BESS}} = K_{\text{depr}}^{\text{bat}}(S_{\text{nom}}^{\text{inv}}, E_{\text{nom}}, P_{\text{nom}}^{\text{dc}}, E_{\text{eff}}, P_k^{\text{c}}) + K_{\text{E}}(S_{p,k}^{\text{inv}}) + K_{\text{fix}}(S_{\text{nom}}^{\text{inv}}, E_{\text{nom}}, P_{\text{nom}}^{\text{dc}}) \quad (1)$$

The mathematical definition of the cost components is provided in [9]. Two observations are used in the objectives of the optimisation problem. $U_{p,i,k}$ denotes the complex line-to-neutral voltage at connection i on phase p at time step k, obtained by numerical linearisation of the load flow in each time step in each phase relative with reference to the no-BESS scenario. $S_{p,k}^{\text{tot}}$ denotes the grid total complex power consumption at each time step k

$$S_{p,k}^{\text{tot}} = \underbrace{P_{p,k}^{\text{inv}} + \text{j}Q_{p,k}^{\text{inv}}}_{\text{BESS power}} + \underbrace{P_{p,k}^{\text{grid}} + \text{j}Q_{p,k}^{\text{grid}}}_{\text{Grid losses}} + \underbrace{\sum_{h \in \mathcal{H}_{\text{p}}} P_{h,k}}_{\text{Household consumption}} \quad (2)$$

where $\mathcal{H}_{\text{p}}$ is the subset of profiles $\mathcal{H}_0$ connected to phase p. Four connections i are selected along the feeder, as feedback points where the three-phase indoor terminal voltage is measured. These connections are grouped in the set {1, 13, 18, 29}. On the basis of the $U_{p,i,k}$ and $S_{p,k}^{\text{tot}}$, two objectives are defined for peak shaving and voltage regulation of daily extreme values

$$S_{\text{rms}}^{\text{daypeak}} = \sqrt{\frac{1}{n_d}\sum_{d=1}^{n_d} \max_{\substack{k \in \mathcal{K}_d, \\ p \in \{a,b,c\}}} \left|S_{p,k}^{\text{tot}}\right|^2} \quad (3)$$

$$U_{\text{rms}}^{\text{daypeak}} = \sqrt{\frac{1}{n_d}\sum_{d=1}^{n_d} \max_{\substack{k \in \mathcal{K}_d, \\ i \in \{1,13,18,29\}, \\ p \in \{a,b,c\}}} (|U_{p,i,k}| - U_{\text{nom}})^2} \quad (4)$$

where $\mathcal{K}_d$ is the set of time steps in day d. The total cost K_{BESS} is used as a third objective. Voltage and peak power limits are treated as objectives, not as constraints. Owing to the rms index formulation and the maximum value operator, extreme peaks are emphasised. However, it can be very expensive to reduce all peaks, and tolerating some peaks can prove beneficial. There will not be an immediate impact when marginally exceeding certain equipment ratings. Exceeding the transformer apparent power limit will accelerate aging, but will not cause an immediate outage. Therefore the results illustrate how much operational margin a BESS can create, but it not necessarily has to operate to such extent.

4.2 Inverter

The BESS inverter complex power profile $S_{p,k}^{\text{inv}}$ in each phase p is limited by the inverter rating $S_{\text{nom}}^{\text{inv}}$

$$|S_{p,k}^{\text{inv}}| \leq (S_{\text{nom}}^{\text{inv}}/3) \quad \forall p \in \{a, b, c\} \quad (5)$$

Real current limits depend on inverter design details and the instantaneous voltage unbalance, but are assumed to always be higher than this modelled safety limit. The inverter transfers power $S_{p,k}^{\text{inv}}$ between the grid and the batteries P_k^{bat}. Losses are incurred independent of use because of the ρ_{sb} (Table 2) and as a function of use proportional to the apparent power flow $\left|S_{p,k}^{\text{inv}}\right|$. The power balance therefore is

$$\overbrace{P_k^{\text{bat}}}^{\text{Batteries}} = \overbrace{\underbrace{\rho_{\text{sb}} S_{\text{nom}}^{\text{inv}}}_{\text{standby cons.}} + \sum_{p \in \{a,b,c\}} \left(\underbrace{P_{p,k}^{\text{inv}}}_{\text{Active power flow}} + \underbrace{(1 - \eta_{\text{inv}})|S_{p,k}^{\text{inv}}|}_{\text{Flow losses}} \right)}^{\text{Inverter}} \quad (6)$$

Four three-phase inverter designs (Inv_1, Inv_2, Inv_3 and Inv_4) are considered and illustrated in Fig. 3. The general inverter complex

Table 2 Li-ion BESS parameters

Inverter efficiency	η_{inv}	97%
Inverter losses relative to nominal power	ρ_{sb}	10 W/kVA
Inverter specific price	$c_{\text{S}}^{\text{inv}}$	230 €/kVA
Inverter lifetime	$\tau_{\text{P}}^{\text{inv}}$	10 a
Battery charge efficiency	η_{c}	88.2%
Battery discharge efficiency	η_{d}	98.0%
Battery cycle life at $E_{\text{eff}}/E_{\text{nom}} = 80\%$	$n_{(80\%)}$	3000–
Cycle life exponent	q	−1.825 –
Battery charge power-to-energy ratio	γ_{c}	1 h^{-1}
Battery discharge power-to-energy ratio	γ_{d}	4 h^{-1}
Battery specific price	$c_{\text{E}}^{\text{bat}}$	1000 €/kWh
Battery nominal power specific investment	$c_{\text{P}}^{\text{bat}}$	270 €/kW
Battery peripherals lifetime	$\tau_{\text{P}}^{\text{bat}}$	10 a
Battery shelf life	$\tau_{\text{E,sl}}^{\text{bat}}$	10 a

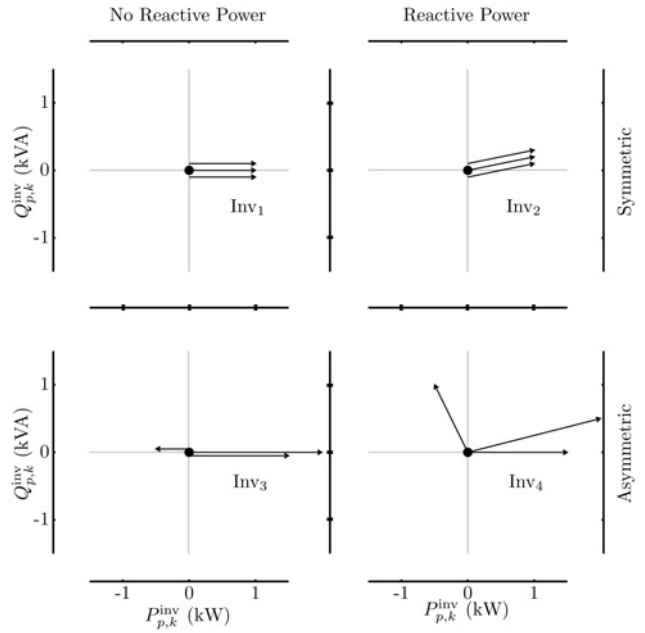

Fig. 3 *Active and reactive powers in each of the phases of the four inverter models while discharging the battery at about 3 kW*

(Individual phase vectors displayed slightly offset for illustrative purposes.)

output power in phase p at time step k is given by

$$S^{\text{inv}}_{p,k} = P^{\text{inv}}_{p,k} + \text{j}Q^{\text{inv}}_{p,k} \quad \forall p \in \{a, b, c\} \tag{7}$$

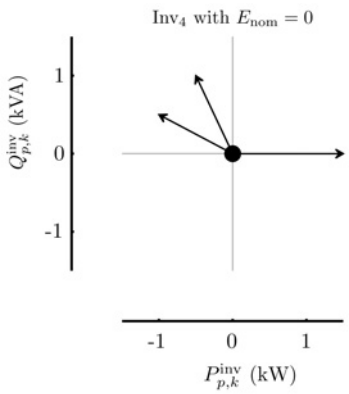

Fig. 4 *Asymmetric inverter, even without batteries, can provide active power transfer between phases, however, it remains a net consumer because of losses*

The first inverter only allows symmetric active power exchange with the grid; the second inverter model adds reactive power exchange; the third inverter model controls the active power in each phase independently, without reactive power exchange; the final inverter model is capable of providing active and reactive powers, for each phase individually. Such functionality requires three single-phase inverters with a common dc bus or one three-phase four-wire inverter [21]. The inverter designs x_{inv} are part of the set $\mathcal{X}_{\text{inv}} = \{\text{Inv}_1, \text{Inv}_2, \text{Inv}_3, \text{Inv}_4\}$. The inverter complex power in phase p at time step k is

$$\text{Inv}_1 : S^{\text{inv}}_{a,k} = S^{\text{inv}}_{b,k} = S^{\text{inv}}_{c,k} = P^{\text{inv}}_{k} \tag{8}$$

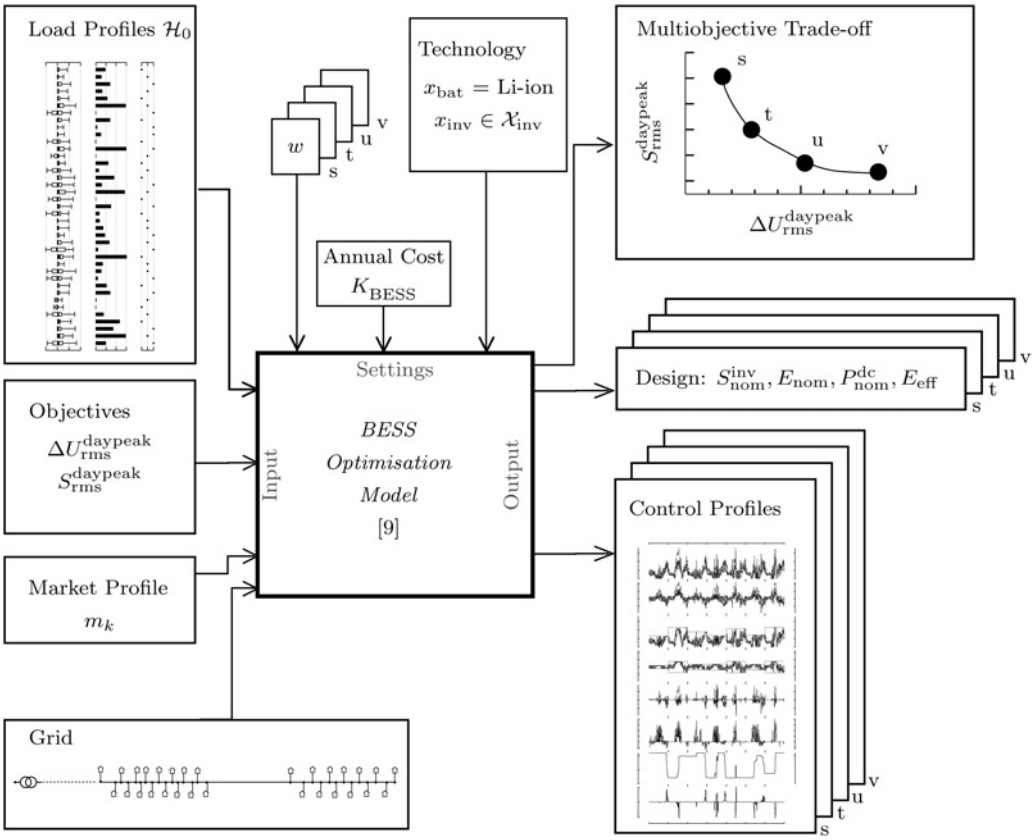

Fig. 5 *Simulation approach: load profiles, objectives, market profile and grid topology as inputs, and design parameters, control profiles and a trade-off curve as output*

Weights $w \in \{s, t, u, v\}$ indicate points used to calculate the trade-off curve

IET Gener. Transm. Distrib., 2015, Vol. 9, Iss. 10, pp. 929–936

$$\text{Inv}_2\colon S_{a,k}^{\text{inv}} = S_{b,k}^{\text{inv}} = S_{c,k}^{\text{inv}} = P_k^{\text{inv}} + \text{j}Q_k^{\text{inv}} \tag{9}$$

$$\text{Inv}_3\colon S_{p,k}^{\text{inv}} = P_{p,k}^{\text{inv}}, \quad \forall p \in \{a, b, c\} \tag{10}$$

$$\text{Inv}_4\colon S_{p,k}^{\text{inv}} = P_{p,k}^{\text{inv}} + \text{j}Q_{p,k}^{\text{inv}}, \quad \forall p \in \{a, b, c\} \tag{11}$$

The power balance at the grid side is maintained by charging and discharging the battery. Nevertheless, even without batteries, the inverter can inject active power into the grid in one or two phases, which is provided by the other (two) phase(s) (Fig. 4).

4.3 Battery

The battery model is maintained from [9]. The battery energy content E_k at time step k, satisfies the recurrence relation (12), where T_s is the

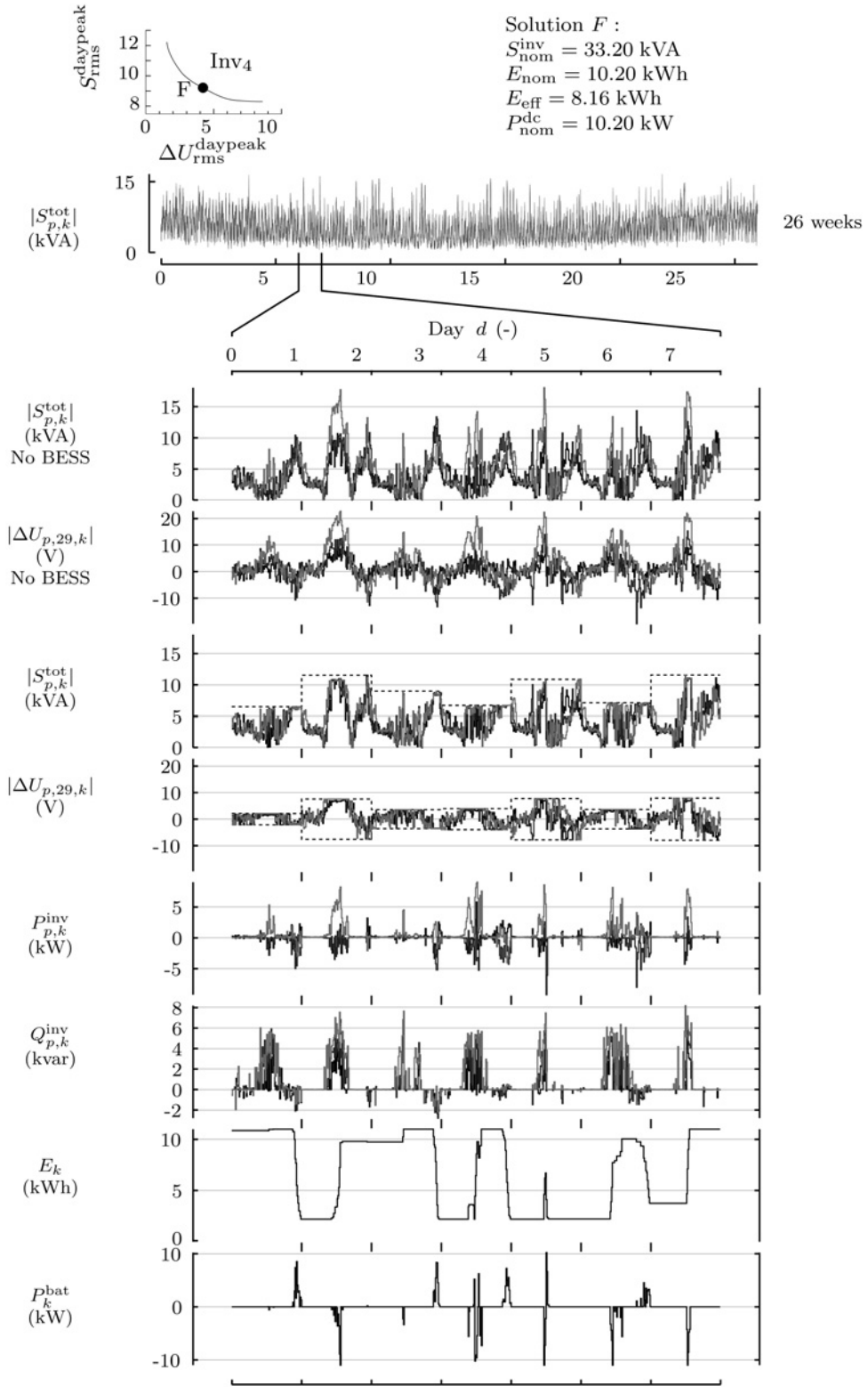

Fig. 6 *Grid impact and BESS decision variables for control of an Inv$_4$-based optimum (solution F), shown for a single week out of the 26 week simulation horizon*

Individual phase values are depicted with varying grey-scale values

time step and η_c and η_d the discharge efficiency, respectively. Initially, the battery is charged to 50% of the usable capacity and at the last time step, the battery must have an equal or higher energy content (13). The effective battery capacity E_{eff} limits the battery energy content (14). The ratio E_{eff}/E_{nom} is between 5 and 80%

$$E_k = E_{k-1} + \eta_c T_s P_k^c - \frac{1}{\eta_d} T_s P_k^d \tag{12}$$

$$E_0 = \frac{1}{2} E_{eff}, \quad E_{n_t} \geq \frac{1}{2} E_{eff} \tag{13}$$

$$0 \leq E_k \leq E_{eff} \leq E_{nom}, \quad 0.05 \leq \frac{E_{eff}}{E_{nom}} \leq 0.8 \tag{14}$$

Charge power P_k^c and discharge power P_k^d at any time step k are defined as separate variables. Limits on charge and discharge powers are imposed because of the dc link with the inverter (15), and the battery technology (16). Factors γ_c, γ_d represent the power-to-energy ratio during charging and discharging for the battery technology. Finally, charging and discharging at the same time is not feasible (17)

$$0 \leq P_k^c \leq P_{nom}^{dc}, \quad 0 \leq P_k^d \leq P_{nom}^{dc} \tag{15}$$

$$P_k^c \leq \gamma_c E_{nom}, \quad P_k^d \leq \gamma_d E_{nom} \tag{16}$$

$$P_k^{bat} = P_k^d - P_k^c, \quad P_k^c P_k^d = 0 \tag{17}$$

4.4 Parameters

The set of parameters is maintained from previous work [9], based on [30]. The inverter parameters are listed in Table 2. No distinction is made in the cost of the different inverter designs, as no reliable price differences are found in the very limited market of battery inverters with the modelled capabilities. Therefore, the results will show the benefit of the added functionality, but may not fully reflect the cost.

The Li-ion battery technology (x_{bat} = Li-ion) parameters used are listed in Table 2. During operation, the nominal capacity and the internal resistance of a battery change [31]. Consequently, even when considering maintenance, the cost structure of the BESS will change. For instance, the increasing internal resistance impacts the charging efficiency, which will in turn increase the energy cost component. Such uncertainties can be assessed through a multiyear simulation horizon, but this is considered out of the scope of this work.

The grid energy loss per time step E_{loss}^{grid} is determined through load flow [28] of the result of the multi-objective optimisation. The BESS internal energy loss per time step E_{loss}^{BESS} is the sum of the inverter losses, which include standby losses and apparent power proportional losses, and the battery losses, which occur during charging and discharging

$$E_{loss}^{BESS} = E_{loss}^{inv} + E_{loss}^{batt} \tag{18}$$

$$E_{loss}^{inv} = \frac{1}{n_t} \sum_{k=1}^{n_t} \sum_{p \in \{a,b,c\}} ((1 - \eta_{inv}) |S_{p,k}^{inv}| + \rho_{sb} S_{nom}^{inv}) \tag{19}$$

$$E_{loss}^{batt} = \frac{1}{n_t} \sum_{k=1}^{n_t} \left((1 - \eta_c) P_k^c + \left(\frac{1 - \eta_d}{\eta_d} \right) P_k^d \right) \tag{20}$$

4.5 Multi-objective optimisation model

$$\begin{array}{ll} \text{minimise} & w \cdot \left(\dfrac{\Delta U_{rms}^{daypeak}}{\Delta U_0} \right)^2 + (1 - w) \cdot \left(\dfrac{S_{rms}^{daypeak}}{S_0} \right)^2 \\ \text{decision var.} & S_{nom}^{inv}, E_{nom}, E_{eff}, P_{nom}^{dc}, S_{p,k}^{inv} \\ \text{subject to} & K_{BESS} \leq 5000\,€/\text{a} \\ & \text{BESS model [9], (18)} \\ & \text{Scenario } \textit{Section } 3 \end{array} \tag{21}$$

A multi-objective optimisation problem in (1), (3) and (4) is stated in (21). The objectives are normalised by the reference objective values without BESS (ΔU_0, S_0). This formulation treats voltage and apparent power limits as soft constraints for a given maximum annual cost.

Fig. 5 details the approach followed in this paper. Four inputs are used for the optimisation model: the load profile set $\mathcal{H}_0$, the grid model, the market profile and the objectives. The multi-objective problem is reduced to a set of single-objective problems with varying objective weights w. For each of the underlying single-objective problems, a set of design parameters and a set of control profiles is obtained. These weights correspond to individual points calculated on the trade-off curves. For each

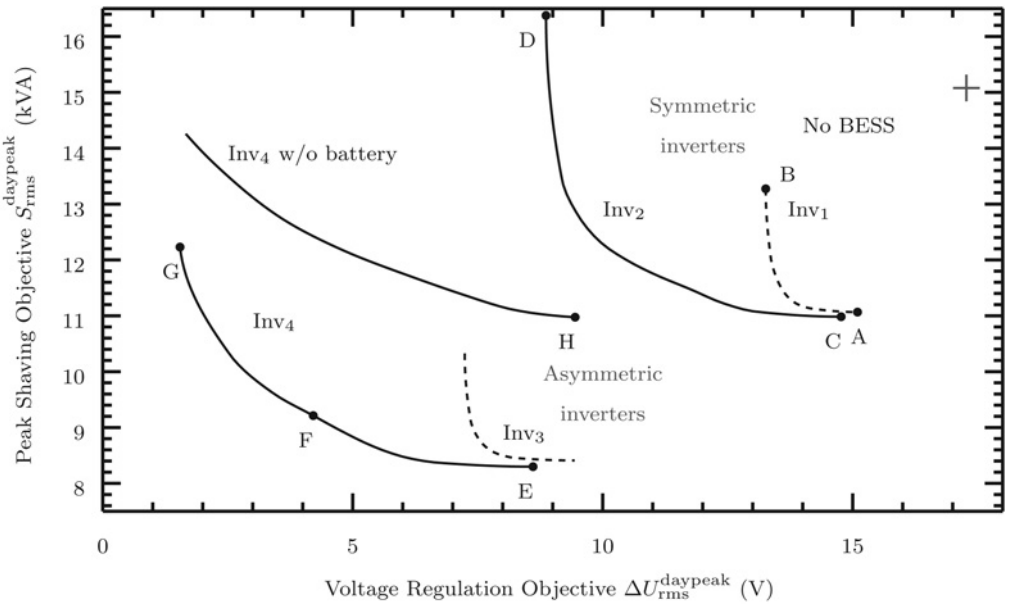

Fig. 7 *Isocost trade-off curves for Li-ion BESS of 5000 €/a with different inverter models*

IET Gener. Transm. Distrib., 2015, Vol. 9, Iss. 10, pp. 929–936

point, there is a corresponding sizing of the BESS, as indicated by the design values $S^{\text{inv}}_{\text{nom}}$, E_{nom}, $P^{\text{dc}}_{\text{nom}}$ and E_{eff}. Furthermore, for each point there are corresponding control time profile results, which illustrate the operation of the BESS in the grid. This approach is repeated to determine the trade-off curves for all inverter designs $x_{\text{inv}} \in \mathcal{X}_{\text{inv}} = \{\text{Inv}_1, \text{Inv}_2, \text{Inv}_3, \text{Inv}_4\}$.

The SQP optimisation model [9] is solved in Yalmip [32] and with the ILOG CPLEX solver. Up to five SQP iterations are needed to optimise the original NLP, by approximating the nonlinear constraint on cyclelife (involving $E_{\text{eff}}/E_{\text{nom}}$) in each iteration. The grid load flow is numerically linearised for each time step independently, in the reference operating point. After the optimisation is solved, the obtained complex power profile of the BESS is used to validate the load flow results.

The chosen inverter design impacts the number of decision variables in the optimisation problem. Each time step, in the simulation horizon has only a single control variable in case of Inv_1; Inv_2 has 2; Inv_3 has 3; Inv_4 has 6. To decrease the solver time for long horizon simulations, an equality constraint on the battery energy content E_k is added every four weeks

$$E_k = \frac{1}{2}E_{\text{eff}}, \quad k \in \mathcal{K}_{m,0} \tag{22}$$

where $\mathcal{K}_{m,0}$ is the set of indices of the first time step of each fourth week. The impact of this constraint on the optimal solution is negligible in case of frequent cycling.

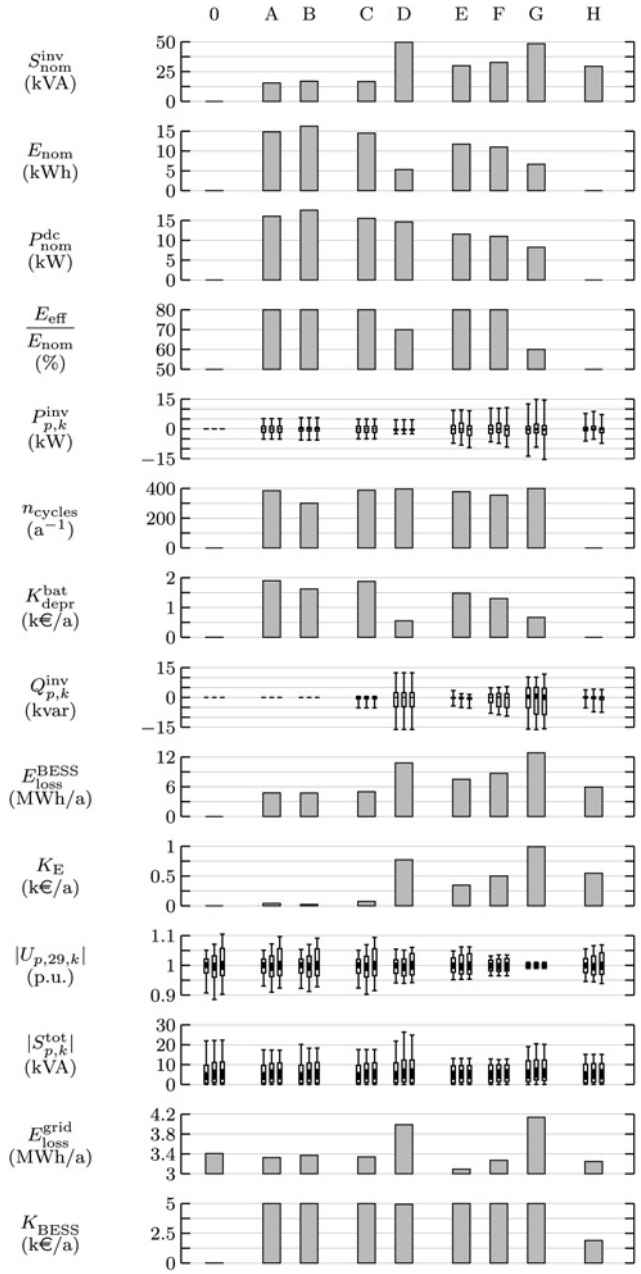

Fig. 8 *Design variables and performance indicators for the solutions A–H in Fig. 7*

5 Results

In all the results, the BESS annual cost is fixed at 5000 €/a and it is connected directly to the feeder at $i = 16$. The lines l thermal constraints $|J_{p,l,k}| < J^{\text{nom}}_{\text{l}}$ do not impact the presented results of the case study. Results which depend on the time horizon of the simulation (of 26 weeks) are presented as annual values to simplify interpretation. Grid impact results are obtained by load flow, which is part of the optimisation model.

5.1 Control with Inv_4

First, a control result of Inv_4 is presented, to illustrate the improvement of both objectives at the same time. A one-week snapshot of the control variables and the resulting grid impact is shown in Fig. 6. In rows 1 and 2, the original time profiles of the transformer apparent power, and the voltage deviations at connection 29 are shown. Rows 3 and 4 show the resulting transformer apparent power and node voltage magnitude values in each phase; the dotted lines represent the resulting daily extreme values of the objectives during BESS operation. Furthermore, rows 5 and 6 show, respectively, the BESS active and reactive power control variables in each phase. Rows 7 and 8 depict the resulting energy content and charge/discharge schedule. It is shown that $P^{\text{inv}}_{p,k}$ differs substantially from P^{bat}_{k}. Sometimes, inter-phase power exchange and reactive power control is sufficient to improve to objectives, at other times battery cycling is required.

5.2 Sizing for different inverter designs

The solutions of the multi-objective sizing problem are presented as isocost trade-off curves between the objectives of peak shaving and voltage control for a fixed maximum annual cost. The trade-off curves indicate the compatibility of the objectives: if one of objective is improved, the other one decreases. Each trade-off curve is a Pareto front with multiple set points for the design variables and control strategy.

The trade-off curves for Inv_1, Inv_2, Inv_3 and Inv_4 are shown in Fig. 7. For both the symmetric and the asymmetric designs, reactive power capabilities (Inv_2, Inv_4) allow for more effective voltage regulation compared to active power only designs (Inv_1, Inv_3). Furthermore, Inv_4 dominates all other designs. Even with an inverter of type Inv_4 without batteries, both objectives are significantly improved compared to Inv_1 and Inv_2, with respect to the solution without BESS. This illustrates the value of inter-phase exchange of active power.

On the trade-off curve points *A*–*H* are marked, however, on each curve ten weights w were calculated to obtain sufficient detail. *A*, *C*, *E* and *H* reflect a high weight for the peak shaving objective; *B*, *D* and *G* reflect a high weight for the voltage regulation objective; point *F* is a knee point and reflects a trade-off strategy between both objectives.

The corresponding decision variables and additional performance indicators are shown in Fig. 8. The depicted parameters are introduced and discussed row by row.

The decision variables for design are shown in rows 1–4. For any objective, Inv_1 has the smallest inverter rating (row 1) and Inv_4 the largest. Conversely, battery capacity (row 2) is highest for Inv_1 and smallest for Inv_4. As can be seen in row 5, active power control is symmetric for Inv_1 and Inv_2. The designed-for peak shaving BESSs (points *A*, *C* and *E*) cause the highest battery

cycling rates (row 6), with the number cycles defined as the energy which ends up in the battery divided by the usable capacity [9]. Consequently, they have the battery highest depreciation cost (row 7) as defined by $K_{\text{depr}}^{\text{bat}} = c_{\text{E}}^{\text{bat}} E_{\text{nom}} / \tau_{\text{E}}^{\text{bat}}$.

The designed-for voltage regulation BESSs (*B*, *D* and *G*) benefit from reactive power control capabilities, as shown in row 8. However, reactive power control increases BESS losses, as shown in row 9, which in turn increases the energy costs, as shown in row 10. Rows 11 and 12, respectively, depict the voltage profile distribution at connection 29 and the apparent power at the transformer. It is shown that the BESS can create a margin to allow the further increase of local consumption or RES. It is seen that the unbalanced inverter designs Inv_3 and Inv_4 manage to equalise the existing voltage unbalance in the peaks. Reactive power control capable inverters only increase the grid losses when used for voltage regulation (row 13). Row 14 shows that the available budget is fully used for all solutions except inverter-only solution *H*. The objectives of *H* cannot be further improved above an annual cost of 1900 €/a, as the transformer power peaks become fully balanced.

On the trade-off curve of Inv_4 a knee-point *F* is marked, as an example of one of the possible solutions between extreme points *E* and *G*. It is noted that Fig. 6 displays a one-week snapshot of knee-point solution *F*. Solution *F* is in design very similar to *E*, however accomplishes more voltage regulation. Compared to *E*, the battery cycling decreases, reactive power is used more often and the BESS losses increase. This strategy change is reflected in the cost components: the depreciation cost decreases and the energy cost increases. Going from *F* to *G* substantially impacts the design: battery capacity is decreased in exchange for a larger inverter.

6 Conclusions

Modelling a BESS purely as a finite source/sink of active power in a LV grid, strongly underestimates the potential because of the existing phase unbalance. Counteracting phase unbalance through an inter-phase power transfer capable inverter, even more so than adding reactive power control, improves the performance of BESSs. However, it substantially increases the number of control variables in the proposed method, which increases solver time. Nevertheless, the results show that it is crucial to take phase unbalance and asymmetric inverter models into account in storage studies in grids where phase unbalance is expected.

The model can be used within grid planning frameworks, such as [33], as it allows to include multiservice strategies explicitly. There, through the formulation of technical control objectives, the corresponding soft constraints could be handled probabilistically.

7 Acknowledgments

This work was supported by the Flemish Government through the LINEAR project (IWT/090800) organized by the Institute for Science and Technology (IWT). Frederik Geth was partially funded by and enrolled in the KIC InnoEnergy PhD School. Jeroen Tant was supported by a Ph.D. fellowship from the Research Foundation – Flanders (FWO).

8 References

1 Whittingham, M.S.: 'History, evolution, and future status of energy storage', *Proc. IEEE*, 2012, **100**, (Special Centennial Issue), pp. 1518–1534
2 Kezunovic, M., McCalley, J.D., Overbye, T.J.: 'Smart grids and beyond: achieving the full potential of electricity systems', *Proc. IEEE*, 2012, **100**, (Special Centennial Issue), pp. 1329–1341
3 Ulbig, A., Andersson, G.: 'On operational flexibility in power systems'. IEEE Power and Energy Society General Meeting, 2012, San Diego, USA, 2012
4 Rastler, D.M.: 'Electric energy storage technology options: a white paper primer on applications, costs, and benefits'. Technical Report 1020676, Electric Power Research Institute, Palo Alto, CA, 2010
5 Manz, D., Piwko, R., Miller, N.: 'Look before you leap', *IEEE Power Energy Mag.*, 2012, **10**, (4), pp. 75–84
6 He, X., Delarue, E., D'haeseleer, W., Glachant, J.-M.: 'A novel business model for aggregating the values of electricity storage', *Energy Policy*, 2011, **39**, (3), pp. 1575–1585
7 Braun, M., Stetz, T.: 'Multifunctional photovoltaic inverters economic potential of grid-connected multifunctional PV-battery-systems in industrial environments'. Twenty-Third Photovoltaic Solar Energy Conf., Valencia, Spain, September 2008, pp. 1–8
8 Geth, F., Tant, J., De Rybel, T., Tant, P., Six, D., Driesen, J.: 'Techno-economical and life expectancy modeling of battery energy storage systems'. Twenty-First Int. Conf. Exhibition Electricity Distribution, Frankfurt, Germany, 2011, vol. 1106
9 Tant, J., Geth, F., Six, D., Tant, P., Driesen, J.: 'Multiobjective battery storage to improve PV integration in residential distribution grids', *IEEE Trans. Sustain. Energy*, 2013, **4**, (1), pp. 182–191
10 Xu, Y., Singh, C.: 'Multi-objective design of energy storage in distribution systems based on modified particle swarm optimization'. IEEE Power and Energy Society General Meeting, San Diego, USA, 2012, pp. 1–8
11 Geth, F., Tant, J., Haesen, E., Driesen, J., Belmans, R.: 'Integration of energy storage in distribution grids'. IEEE Power and Energy Society General Meeting, Minneapolis, MN, 2010, pp. 1–6
12 Oh, H.: 'Optimal planning to include storage devices in power systems', *IEEE Trans. Power Syst.*, 2011, **26**, (3), pp. 1118–1128
13 Atwa, Y.M., El-Saadany, E.F.: 'Optimal allocation of ESS in distribution systems with a high penetration of wind energy', *IEEE Trans. Power Syst.*, 2010, **25**, (4), pp. 1815–1822
14 Doughty, D.H., Butler, P.C., Akhil, A.A., Clark, N.H., Boyes, J.D.: 'Batteries for large-scale stationary electrical energy storage', *Electrochem. Soc. Interface*, 2010, **19**, (3), pp. 49–53
15 Chakraborty, S., Senjyu, T., Toyama, H., Saber, A., Funabashi, T.: 'Determination methodology for optimising the energy storage size for power system', *IET Gener. Transm. Distrib.*, 2009, **3**, (11), p. 987
16 Delghavi, M.B., Yazdani, A.: 'A unified control strategy for electronically interfaced distributed energy resources', *IEEE Trans. Power Deliv.*, 2012, **27**, (2), pp. 803–812
17 Barnes, A.K., Balda, J.C., Escobar-meja, A., Geurin, S.O.: 'Placement of energy storage coordinated with smart PV inverters'. IEEE PES Innovative Smart Grid Technologies, Washington DC, USA, 2012, pp. 1–7
18 Gabash, A., Li, P.: 'Active-reactive optimal power flow for low-voltage networks with photovoltaic distributed generation'. Second IEEE Energycon Conf. Exhibtion, 2012, pp. 381–386
19 Gabash, A., Li, P.: 'Flexible optimal operation of battery storage systems for energy supply networks', *IEEE Trans. Power Syst.*, 2013, **28**, (3), pp. 2788–2797
20 Song, Y., Zhang, F., Hu, Z.: 'Mixed-integer linear model for transmission expansion planning with line losses and energy storage systems', *IET Gener. Transm. Distrib.*, 2013, **7**, (8), pp. 919–928, URL http://www.digital-library.theiet.org/content/journals/10.1049/iet-gtd.2012.0666
21 Aredes, M., Hafner, J., Heumann, K.: 'Three-phase four-wire shunt active filter control strategies', *IEEE Trans. Power Electron.*, 1997, **12**, (2), pp. 311–318
22 Nourai, A., Sastry, R.: 'A vision & strategy for deployment of energy storage in electric utilities'. IEEE Power and Energy Society General Meeting, 2010, pp. 1–4
23 Weckx, S., Gonzalez, C., Tant, J., De Rybel, T., Driesen, J.: 'Parameter identification of unknown radial grids for theft detection'. IEEE PES Innovative Smart Grid Technologies, Berlin, Germany, 2012, pp. 1–6
24 'Kabels voor ondergrondse aanleg, met synthetische isolatie en versterkte mantel (type 1kv)', 1975
25 De Brabandere, K., Bolsens, B., Van den Keybus, J., Woyte, A., Driesen, J., Belmans, R.: 'A voltage and frequency droop control method for parallel inverters', *IEEE Trans. Power Electron.*, 2007, **22**, (4), pp. 1107–1115
26 Dupont, B., Vingerhoets, P., Tant, P., *et al.*: 'LINEAR breakthrough project: large-scale implementation of smart grid technologies in distribution grids'. IEEE PES Innovative Smart Grid Technologies, Berlin, Germany, 2012
27 Labeeuw, W., Deconinck, G.: 'Customer sampling in a smart grid pilot'. IEEE Power and Energy Society General Meeting, San Diego, USA, 2012, pp. 1–7
28 Cheng, C., Shirmohammadi, D.: 'A three-phase power flow method for real-time distribution system analysis', *IEEE Trans. Power Syst.*, 1995, **10**, (2), pp. 671–679
29 'Voltage characteristics of electricity supplied by public electricity networks', July 2010
30 'WP1.3 Parameter Manual', (2010), URL www.g4v.eu
31 Dogger, J.D., Roossien, B., Nieuwenhout, F.D.J.: 'Characterization of Li-ion batteries for intelligent management of distributed grid-connected storage', *IEEE Trans. Energy Convers.*, 2011, **26**, (1), pp. 256–263
32 Löfberg, J.: 'YALMIP: A toolbox for modeling and optimization in MATLAB'. 2004 IEEE Int. Symp. Computer Aided Control System Design, Taipei, Taiwan, 2004, pp. 284–289
33 Alarcon-rodriguez, A., Haesen, E., Ault, G., Driesen, J., Belmans, R.: 'Multi-objective planning framework for stochastic and controllable distributed energy resources', *IET Renew. Power Gener.*, 2009, **3**, (2), pp. 227–238